Inelastic Atomic Scattering of 0.1-, 0.2-, 0.4-, and 3.0-MeV Electrons*

G. Missoni,† C. E. Dick, R. C. Placious, and J. W. Motz
National Bureau of Standards, Washington, D.C. 20234
(Received 6 July 1970)

Spectral data obtained with a magnetic spectrometer are presented for inelastic electron scattering from thin targets of carbon, copper, and gold at incident electron energies of 0.1, 0.2, 0.4, and 3.0 MeV, for scattering angles between 20° and 120°. For angles less than 90°, each spectrum consists of (a) a Møller line which has a half-width that increases with atomic number and which yields an experimental cross section that agrees within experimental error with the theoretical Møller cross section, and (b) a low-energy continuum which rises steeply at energies less than 40 keV. For angles greater than 90°, the Møller line which is kinematically forbidden vanishes, but the steeply rising continuum remains. This continuum may arise from single electron-atom scattering and from multiple scattering in the target. The latter process depends on target thickness. The experimental results for this low-energy continuum tend to confirm that the multiple-scattering effects as calculated by Ford and Mullin dominate the single-scattering process as calculated by Weber, Deck, and Mullin, and by Kolbenstvedt and Cooper even for an 11-$\mu g/cm^2$ carbon target which was the most favorable case for studying the single-scattering process. Because of multiple scattering, accurate experimental data for the low-energy continuum produced by single electron-atom inelastic scattering can best be obtained with gas targets.

I. INTRODUCTION

Studies of inelastic electron scattering by atoms have been carried out in the nonrelativistic region (< 1 keV), where the kinetic energy of the incident electron is comparable to the atomic-binding energies.[1] These studies are generally carried out with gas targets to minimize solid-state binding effects and the emphasis has been on total and not differential scattering measurements. At these low energies, the dominant inelastic scattering process involves atomic excitation and ionization effects. As the incident electron energy increases to the relativistic region, the effect of atomic binding becomes less important, and the electron-scattering process approaches the condition of direct interactions with the atomic electrons and nucleus.

At extremely relativistic energies (> 10 MeV), the main contribution to inelastic electron scattering is estimated by electron-electron or Möller[2] scattering for free electrons. In the intermediate region, where the incident electron energies are between approximately 0.1 and 3.0 MeV as in the present measurements, and where the electron-scattering angles are larger than 20°, the main contribution to inelastic electron scattering is still estimated by Möller scattering for free electrons. However, atomic-binding effects are important in this intermediate region and must be accounted for to explain large-angle inelastic scattering, particularly at angles larger than 90° where Möller scattering is kinematically forbidden for the case in which the target electron is initially at rest in the laboratory system.

Very few theoretical treatments of inelastic electron scattering by atoms are available that apply to the intermediate energy region (of the order of the electron rest energy) and that can predict the energy and angular distributions of the scattered electrons. Among the pertinent studies, Ford and Mullin,[3] and Weber, Deck, and Mullin[4] have calculated the K-ionization cross-section differential with respect to the energy and angle of the scattered electrons, with approximations that apply to large scattering angles and to initial electron energies that are large compared to the electron rest energy. Otherwise, the available calculations[1] that account for atomic-binding effects apply to the nonrelativistic energy region.

Previous experimental studies of inelastic electron scattering in the intermediate energy region at scattering angles of 100°[5] at incident energy of 500 keV and at angles of 40°, 90°, 120°, and 140°[6] at 200 and 400 keV. The 500-deV measurements have shown the inadequacy of the Weber, Deck, and Mullin calculations[4] of inelastic electron spectra for the intermediate electron energies. In both studies, the mediate electron energies. In both studies, the experimental results show that the inelastic electron spectra are continuous over most of the low-energy region. These inelastic spectra are superimposed on the Moller lines for scattering angles less than 90° and have intensities that are considerably larger than the Weber, Deck, and Mullin predictions.

The present study was undertaken to obtain more accurate data on the energy distribution of inelastically scattered electrons in the region from approximately 10 to 400 keV, and to help resolve some

of the discrepancies that exist[6] in the comparisons between theory and experiment. Accurate spectral measurements of electrons in this low-energy region are difficult to make because in most experimental conditions there is an appreciable contribution of low-energy electrons which are produced as a result of multiple scattering in the target, in the walls of the scattering chamber, and the edges of the defining slits. As discussed in Sec. II, special design features are introduced in the experimental conditions for the present measurements in order to minimize the contribution of electrons from the above unwanted sources.

The present measurements are carried out with incident electron energies of 0.1, 0.2, 0.4, and 3.0 MeV and with thin targets of carbon, copper, and gold. Spectral distributions of the inelastically scattered electrons are obtained at scattering angles of 20°, 30°, 40°, 60°, 90°, and 120° and extend over the range from approximately 10 to 400 keV.

II. EXPERIMENTAL APPARATUS AND PROCEDURE

In the present experiment, the monoenergetic electron beams are provided with beam diameters of approximately 3 mm by the NBS 0.5- and 4.0-MeV dc accelerators. As shown in Fig. 1, the electron beam which is incident on thin targets is collected by the insulated target chamber and electron trap, and the total incident charge is measured with a current integrator with better than 1% accuracy. The scattered electrons are observed at a given scattering angle θ within a solid angle Ω which is defined by a circular aluminum defining aperture. For scattering angles less and greater than 90°, the scattered electrons are transmitted and reflected respectively by the target which is normal to the electron beam. For 90° scattering, the target is inclined 45° to the beam in the reflection position. In order to reduce the area of the scattering chamber wall which is in the field of view of the detector and which may provide an unwanted source of scattered electrons, an additional antiscatter baffle is inserted between the target and the defining aperture as shown in Fig. 1.

The electrons which are scattered at a given angle from the target contain two components[6]: an elastic component which is produced by electron scattering from the atom[7] and an inelastic component which is produced by atomic ionization and excitation processes. The ratio of the elastic to the inelastic components is of the order of the atomic number of the target, and therefore spurious scattering effects that are produced by the elastic component may seriously distort the energy distribution of the inelastic component. In order to avoid such distortions, it is desirable to suppress the elastically scattered electrons before the spectral measurements are made. In order to achieve this condition, a nondispersive magnet[8] was inserted between the defining aperture and the detector as shown in Fig. 1. This magnet is composed of three rec-

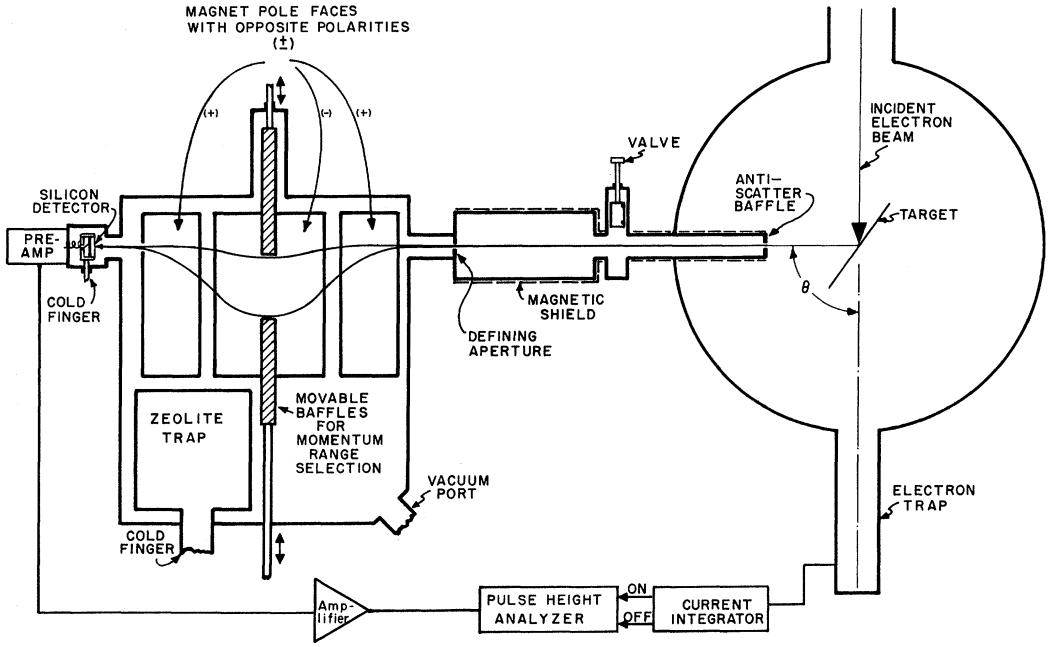

FIG. 1. Experimental arrangement for spectral measurements of electrons inelastically scattered from thin targets of carbon, copper, and gold.

tangular pole faces which produce three approximately equal and alternating magnetic fields.

By properly arranging the intensity of the magnetic fields and the geometry of the baffles in the pole face system, it is possible to select and transmit electrons in particular momentum intervals. Electrons with different momenta are bent along different trajectories which have a maximum separation or dispersion at the middle or symmetry plane of the magnet system and which converge again at the exit of the system to form the transmitted beam. At the symmetry plane of maximum displacement from the direction of the incident beam, there are two movable baffles which can be positioned to select particular momentum intervals. In particular, the baffles can eliminate either the elastic or inelastic components of the beam, and in the former case, they also absorb the photons that are emitted from the target and that may contribute to the distortion of the measured electron spectra. Measurements of the cutoff properties of this system with monoenergetic electron beams indicated that when the elastic peak is removed, the inelastic spectrum is undistorted for energies up to 95% of the elastic energy. These measurements were made by inserting the magnet system in the direct beam from the accelerator and measuring the response of the system to monoenergetic electrons in the energy range 0.10–0.5 MeV. In order to avoid strong defocusing effects and to preserve a good momentum resolution, the beam entering the magnet system must have a small area (of the order of 2 mm^2) and must be carefully collimated and directed. To achieve this accurate geometry, the magnet system, collimation system, and scattering chamber were mounted on a rigid frame and were carefully aligned with a laser beam; in addition, as shown in Fig. 1, magnetic shielding surrounded the electron path from the target to the defining aperture.

The energy distributions of the electrons transmitted through the magnet system are measured with a spectrometer employing a silicon detector (500-μ depletion depth), connected to a low-noise-shaping amplifier and a multichannel analyzer. Because some of the measurements were carried out with the detector at liquid-nitrogen temperature, it was necessary to insert a zeolite trap in the magnet vacuum chamber in order to prevent the condensation of oil vapor on the surface of the detector. The response of the silicon detector to monoenergetic electrons has been described elsewhere[9] and is characterized by a total absorption peak plus a "backscattering" tail which covers the energy region below the peak energy. Measurements with monoenergetic electrons in the region 15–300 keV show that the full width at half-maximum (FWHM) of the total absorption peak is equal to approximately 2 keV, and the ratio of the area under the backscattering tail to the total area is equal to 0.14.[9]

The targets in the present measurements consist of evaporated films of carbon, copper, and gold, and have thicknesses in the range from approximately 10 to 60 $\mu g/cm^2$. The carbon targets are self-supporting with no additional backing material, and the copper and gold targets are evaporated on thin backing films (between 5 and 10 $\mu g/cm^2$) of collodion or carbon. The effect of these backings was accounted for by making measurements on self-supporting foils of the backing material. The average target thickness is determined with an accuracy of approximately 10% from weight and area measurements of the target material. The experimental values for the inelastic cross section, $d^2\sigma/d\Omega dT$, which is differential with respect to the scattered-electron kinetic energy T and solid angle $d\Omega$ is determined from the following equation:

$$\frac{d^2\sigma}{d\Omega dT}=\frac{N}{\Omega nm}\ , \tag{1}$$

where N is the number of scattered electrons per keV interval, Ω is the solid angle subtended by the detector, n is the number of electrons incident on the target, and m is the number of target atoms per cm^2. In these measurements, the distortion in the spectral shapes produced by the response of the detector described above is considered to be negligible compared to other sources of error, and the values for N are determined directly from the pulse-height distributions without introducing unfolding calculations which give corrections for the detector response and which have been described elsewhere.[10]

III. RESULTS AND DISCUSSION

The experimental results show the dependence of the inelastic scattering cross section per atomic electron, $(1/Z)d^2\sigma/d\Omega dT$, on the kinetic energy T of the scattered electron. For incident electron kinetic energies of 400, 200, and 100 keV, Figs. 2–4, respectively, give the experimental cross sections at a scattering angle of 20°, as obtained with thin targets of carbon (61 $\mu g/cm^2$), copper (64 $\mu g/cm^2$ on 10-$\mu g/cm^2$-collodion backing), and gold (50 $\mu g/cm^2$ on 10-$\mu g/cm^2$-collodion backing). For the same respective energies, Figs. 5–7 give the cross sections at a scattering angle of 40° as obtained with thin targets of carbon (33 $\mu g/cm^2$) and gold (55 $\mu g/cm^2$ on 10-$\mu g/cm^2$-collodion backing), and Fig. 8 gives the cross sections at a scattering angle of 60° as obtained with thin targets of gold (9 $\mu g/cm^2$ on 5-$\mu g/cm^2$-collodion backing) and carbon (11 $\mu g/cm^2$).

The first important feature of the inelastic spectra in Figs. 2–8 is the peaks. The peaks are ob-

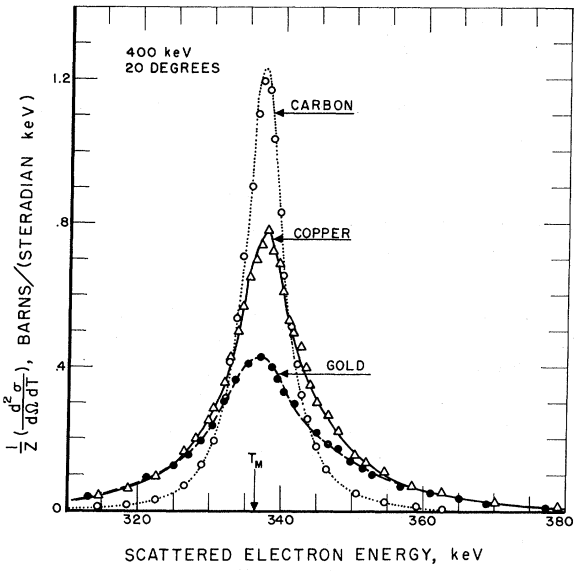

FIG. 2. Inelastic scattering cross sections per atomic electron $(1/Z)d^2\sigma/d\Omega\, dT$ for electron-atomic collisions with an initial-electron kinetic energy of 400 keV and a scattering angle of 20°. Results are given for thin targets of carbon ($Z=6$, 61 $\mu g/cm^2$), copper ($Z=29$, 64 $\mu g/cm^2$), and gold ($Z=79$, 50 $\mu g/cm^2$). For electron-electron collisions (Møller scattering), the kinetic energy T_M of the scattered electron in the laboratory system is indicated by the arrow on the abscissa energy scale.

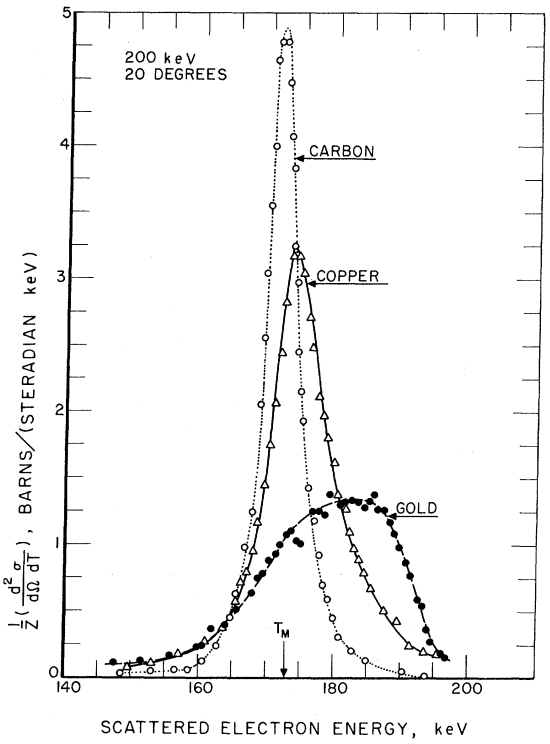

FIG. 3. Inelastic scattering cross sections per atomic electron $(1/Z)\, d^2\sigma/d\Omega\, dT$ for electron-atomic collisions with an initial-electron kinetic energy of 200 keV and a scattering angle of 20°. The targets and the definition of T_M are given in the caption of Fig. 2.

served at scattering angles less than 90° because the scattering conditions approach the case of Møller scattering,[2] and the peaks occur at energies close to the Møller energy T_M which is defined[2] (arrows in figures) by the kinematics in an electron-electron collision in which the target electron is free and at rest in the laboratory system. The observed energy shifts from the predicted Møller[2] energy are not introduced by the energy response of the magnetic-analysis system and may be due to either atomic-binding effects or multiple-scattering effects in the target. As the atomic number of the target increases, these peaks become broader and more distorted because of the increasing influence of atomic-binding effects. Kepes *et al.*[11] have previously observed this broadening of the Møller peaks for low-Z materials for incident electron energies greater than 1 MeV and found qualitative agreement with the predictions of Ford and Mullin[3] for atomic-binding effects. The integrated cross sections obtained from the areas under the peaks agree within experimental error with the Møller cross sections,[2] although the data are not accurate enough (not better than 20% accuracy) to determine whether atomic-binding effects for high-Z targets can introduce differences with the Møller cross-section values.

The second important feature of each of the inelastic spectra in Figs. 2–8 is the continuum on

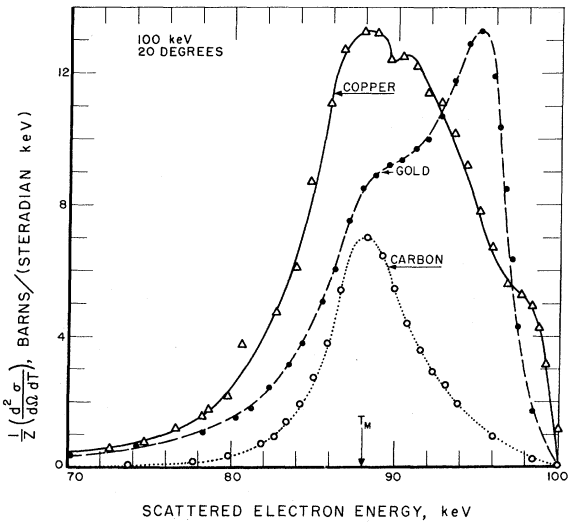

FIG. 4. Inelastic scattering cross sections per atomic electron $(1/Z)\, d^2\sigma/d\Omega\, dT$ for electron-atomic collisions with an initial-electron kinetic energy of 100 keV and a scattering angle of 20°. The targets and the definition of T_M are given in the caption of Fig. 2.

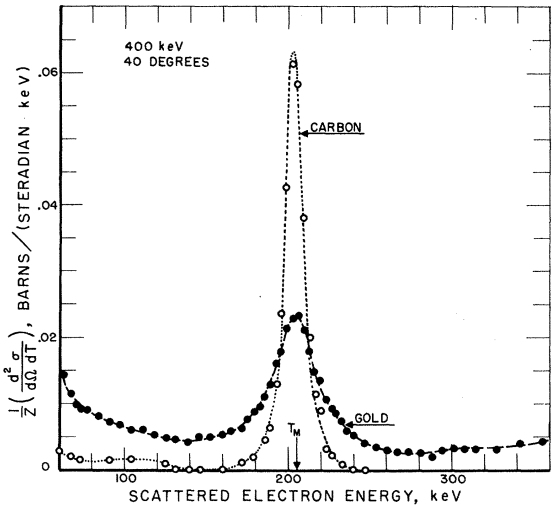

FIG. 5. Inelastic scattering cross sections per atomic electron $(1/Z)\, d^2\sigma/d\Omega\, dT$ for electron-atomic collisions with an initial-electron kinetic energy of 400 keV and a scattering angle of 40°. Results are given for thin targets of carbon ($Z=6$, 33 $\mu g/cm^2$) and gold ($Z=79$, 55 $\mu g/cm^2$). The definition of T_M is given in the caption for Fig. 2.

which the peak is superimposed. This continuum becomes more apparent with prominent components near the extreme energy regions (i.e., near the elastic peak and below 40 keV), as the scattering angle increases from 20° to 60° or as the Møller energy T_M decreases. It is important to determine whether this continuum arises only from the process of single scattering of electrons by atoms.

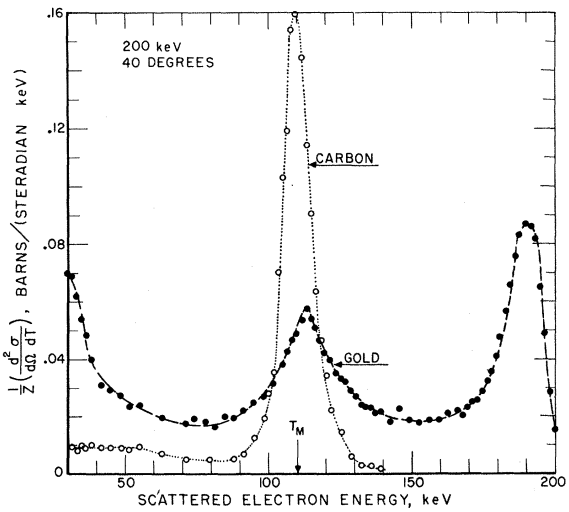

FIG. 6. Inelastic scattering cross sections per atomic electron $(1/Z)\, d^2\sigma/d\Omega\, dT$ for electron-atomic collisions with an initial-electron kinetic energy of 200 keV and a scattering angle of 40°. The targets and the definition of T_M are given in the captions of Figs. 5 and 2, respectively.

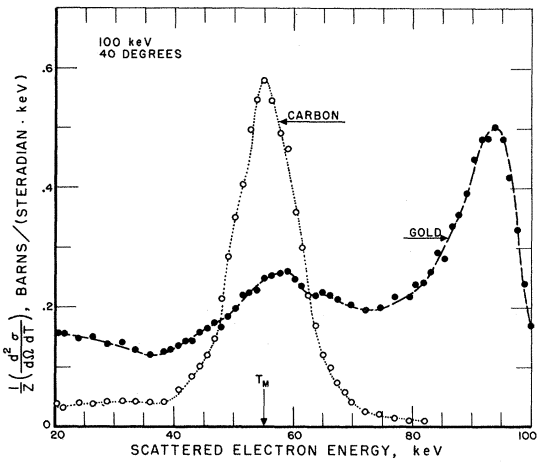

FIG. 7. Inelastic scattering cross sections per atomic electron, $(1/Z)\, d^2\sigma/d\Omega\, dT$ for electron-atomic collisions with an initial-electron kinetic energy of 100 keV and a scattering angle of 40°. The targets and the definition of T_M are given in the captions of Figs. 5 and 2, respectively

Other possible sources for such a continuum are: (i) the bremsstrahlung process, (ii) scattering from walls of the target chamber or the collimation system which are in the field of view of the detector, and (iii) multiple scattering in the target. The contribution of the first source can be neglected because estimates[5,6] of the inelastic electron spectra produced by the bremsstrahlung process give

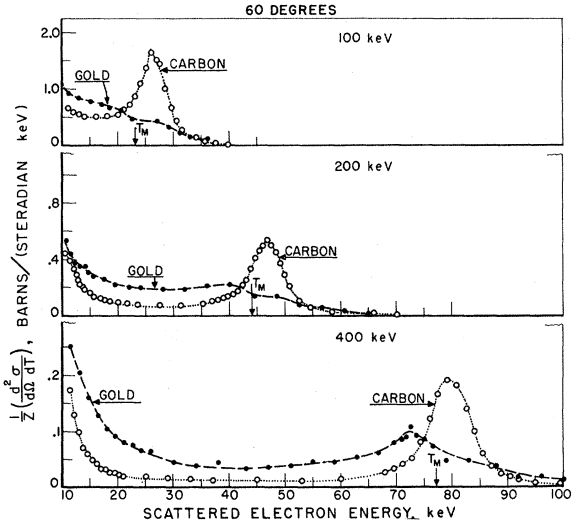

FIG. 8. Inelastic scattering cross sections per atomic electron $(1/Z)\, d^2\sigma/d\Omega\, dT$ for electron-atomic collisions with initial-electron kinetic energies of 100, 200, and 400 keV and a scattering angle of 60°. Results are given for thin targets of carbon ($Z=6$, 11 $\mu g/cm^2$) and gold ($Z=79$, 9 $\mu g/cm^2$), and the definition of T_M is given in the caption of Fig. 2.

cross-section values that are at least an order-of-magnitude smaller than the experimental values for energy losses that are larger than 5 keV. The contribution of the second source was investigated carefully by making spectral measurements with and without the antiscatter baffle (Fig. 1) and with different defining apertures which produced order-of-magnitude changes in the solid angle Ω. The results showed that with no antiscattering baffle and with the larger solid angles used in previous measurements,[6] there are appreciable contributions and changes in the shape of the inelastic spectra from electrons scattered from the walls of the scattering chamber and the collimation system. On the other hand, with the geometry used in the present measurements with an antiscatter baffle and small defining apertures, the contribution of wall scattering is negligible. This result was established by the fact that the spectral shape and the number of scattered electrons per unit solid angle was independent of solid angle for several different apertures which were an order of magnitude smaller than the apertures used in previous measurements.[6] In order to investigate the contributions of multiple scattering to the inelastic spectrum of the scattered electrons, it is necessary to use very-thin targets, particularly for electrons that are emitted from the target with an energy in the region 5–40 keV. The most favorable conditions for such studies can be obtained with thin self-supporting targets having low atomic number, and the results which were obtained for carbon targets are discussed below.

As a test of multiple-scattering effects in the target, spectral measurements for 100-, 200-, and 400-keV electrons scattered at 60° from a carbon target were made for target thicknesses of 11, 23, and 57 $\mu g/cm^2$. The results in Fig. 9 show that as the target thickness increases, the peaks become more distorted and have larger half-widths, and the area under the inelastic continuum increases relative to the area under the peak. Estimates of double scattering in the target as evaluated from Eq. (22) in the Ford-Mullin calculations[3] show that there is an appreciable effect in the energy region above the Møller energy T_M, which may account for the rise in the continuum above this energy that is evident in Figs. 2–8. These results imply that in order to study the inelastic electron spectrum in this energy region for single scattering from targets with high atomic numbers, it is practically necessary to prepare the high-Z targets in the form of atomic beams rather than evaporated foils.

On the basis of the above results, the remaining studies on the inelastic electron spectra were made for the most favorable case with the 11-$\mu g/cm^2$ self-supporting carbon target. Spectral measurements were made at scattering angles of 30°, 60°, 90°, and 120° for scattered electron energies in

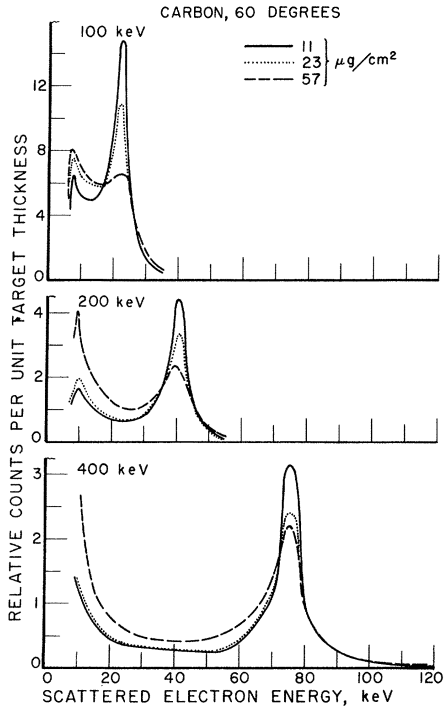

FIG. 9. Dependence of spectral shapes on target thickness, for electrons with initial kinetic energies of 100, 200, and 400 keV inelastically scattered at 60° from 11-, 23-, and 57-$\mu g/cm^2$ carbon targets. The values of T_M are the same as those given in Fig. 8.

the region from approximately 7 to 350 keV for incident electron energies of 0.10, 0.20, 0.40, and 3.0 MeV. The results are shown in Figs. 10–13, respectively.

The data in Figs. 10–13 for the 11-$\mu g/cm^2$ carbon target establish certain features of the inelastic spectra which are similar to the spectral features observed with the thicker carbon, copper, and gold targets in Figs. 2–8. For scattering angles of 30° and 60°, the spectra contain two components: (i) a line that approximates the Møller line produced in direct electron-electron scattering, and (ii) a low-energy continuum below the Møller energy T_M (Fig. 2) that rises sharply for scattered-electron energies below 40 keV. For scattering angles equal to or larger than 90°, the line vanishes and the inelastic spectra contain only the low-energy continuum with the steep slope. It is important to note that such a continuum is present in single electron-atom scattering even for low atomic numbers such as carbon.

From the data in Figs. 10–13, the angular distributions for 10-keV scattered electrons are plotted in Fig. 14 for the incident electron energies of 0.1, 0.2, and 3.0 MeV with the peak values normalized to unity. The results show that as the ratio of the scattered to the incident electron energy de-

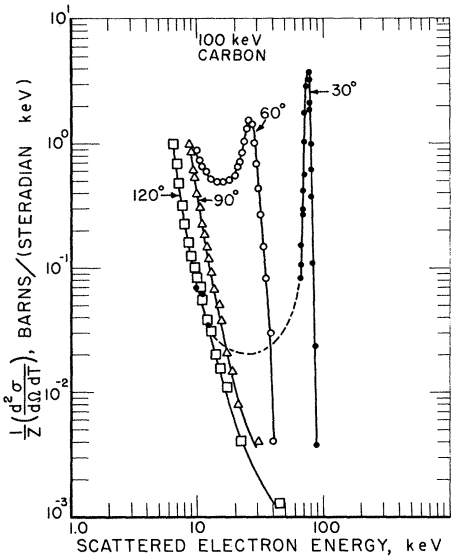

FIG. 10. Inelastic scattering cross sections per atomic electron $(1/Z)\, d^2\sigma/d\Omega\, dT$ for electron-atomic collisions with an initial electron kinetic energy of 0.10 MeV, an 11-μg/cm^2 carbon target, and scattering angles of 30°, 60°, 90°, and 120° .

creases below 0.1, the angular distribution tends to become narrower and to peak at 90°.

Theoretical studies of the inelastic energy spectra for scattered electrons have been made by Ford and Mullin[3] and Weber, Deck, and Mullin.[4] These calculations apply to electrons with initial kinetic

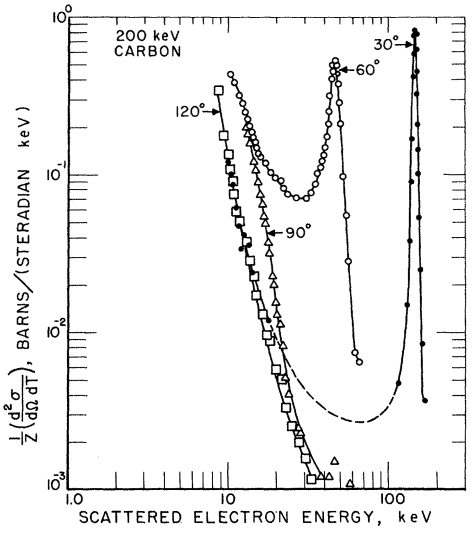

FIG. 11. Inelastic scattering cross sections per atomic electron $(1/Z)\, d^2\sigma/d\Omega\, dT$ for electron-atomic collisions with an initial electron kinetic energy of 0.20 MeV, an 11-μg/cm^2 carbon target, and scattering angles of 30°, 60°, 90°, and 120°.

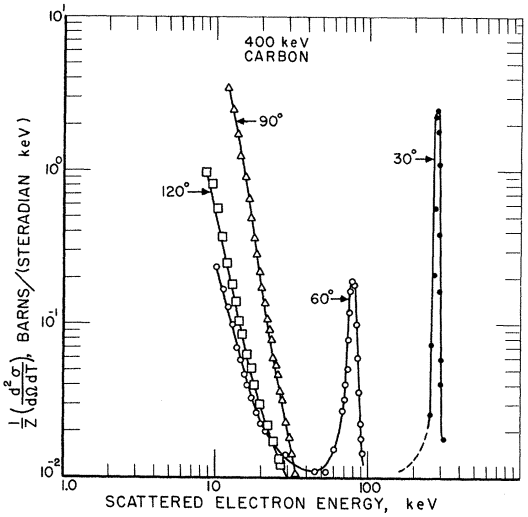

FIG. 12. Inelastic scattering cross sections per atomic electron $(1/Z)\, d^2\sigma/d\Omega\, dT$ for electron-atomic collisions with an initial electron kinetic energy of 0.40 MeV, an 11-μg/cm^2 carbon target, and scattering angles of 30°, 60°, 90°, and 120°.

energies that are large compared to the electron rest energy and that are scattered at angles greater than 90° and include only contributions from the K shell. Ford and Mullin[3] used a nonrelativistic hydrogenlike wave function for the bound electron,

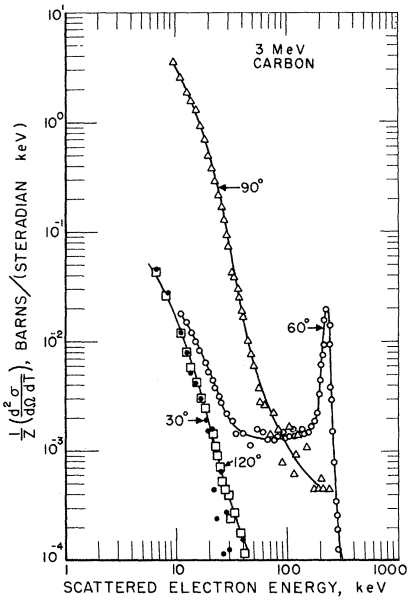

FIG. 13. Inelastic scattering cross sections per atomic electron $(1/Z)\, d^2\sigma/d\Omega\, dT$ for electron-atomic collisions with an initial electron kinetic energy of 3.0 MeV, 11 $-$ μg/cm^2 carbon target, and scattering angles of 30°, 60°, 90°, and 120°. Because of the compressed energy scale, the Møller peak at 30° and the elastic peak are off scale.

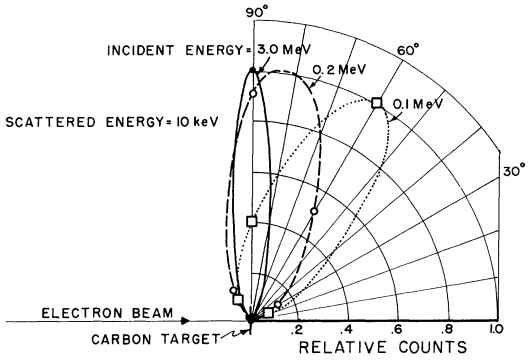

FIG. 14. Angular distributions of 10-keV electrons emitted from an 11-μg/cm^2 carbon target with incident electron kinetic energies of 0.1, 0.2, and 3.0 MeV. These data were obtained from Figs. 10–13, and the peaks in the angular distributions have been normalized to unity.

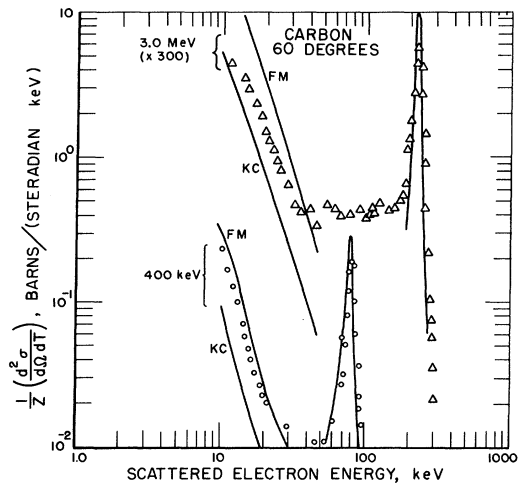

FIG. 15. Comparison of experimental and theoretical inelastic cross sections per atomic electron $(1/Z)\, d^2\sigma/d\Omega\, dT$ for an 11-μg/cm^2 carbon target at 60°, with incident electron energies of 3.0 MeV and 400 keV. The theoretical curves have been evaluated by Kolbenstvedt and Cooper (KC) (Ref. 11), and from Eq. (22) given by Ford and Mullin (FM) (Ref. 3) for multiple scattering. The Møller peaks are those calculated from Kolbenstvedt and Cooper.

and plane-wave functions for the incident and outgoing electrons. Weber, Deck, and Mullin[4] recalculated the cross section in the first Born approximation by including first-order corrections of relativistic Coulomb effects on the bound electron and the low-energy outgoing electron and by neglecting the atomic-binding energy.

In addition to the single-scattering process, Ford and Mullin[3] have made calculations of the effects of multiple scattering where the K ionization process is followed by a nuclear elastic scattering. This calculation is restricted to cases where the incident energy is large compared with the electron rest energy and where the electrons are normally incident on the scattering foil.

Recently, Kolbenstvedt and Cooper[12] have carried out plane-wave calculations for inelastic electron scattering which includes contributions from all atomic shells. These calculations can be expected to be valid at all angles, provided that the initial and scattered-electron energies are high enough to satisfy the Born approximation. Based on the plane-wave approximation [see Eq. (8) of Ref. 3], Kolbenstvedt and Cooper have evaluated the inelastic cross sections for the scattering of 0.4- and 3.0-MeV electrons from thin carbon targets. Comparisons of the experimental results with the cross sections predicted by Kolbenstvedt and Cooper[12] (KC) and by Weber, Deck, and Mullin[4] (WDM), [Eq. (25) of Ref. 4] and Ford and Mullin (FM) for multiple scattering [Eq. (22) of Ref. 3], are given in Figs. 15 and 16, for scattering angles of 60°, and 90° and 120°, respectively.

As can be seen from these figures, there is fair agreement with the FM multiple-scattering calculation for this thin carbon target (11 μg/cm^2 = 5.51 $\times 10^{17}$ carbon atoms/cm^2) and this contribution domi-

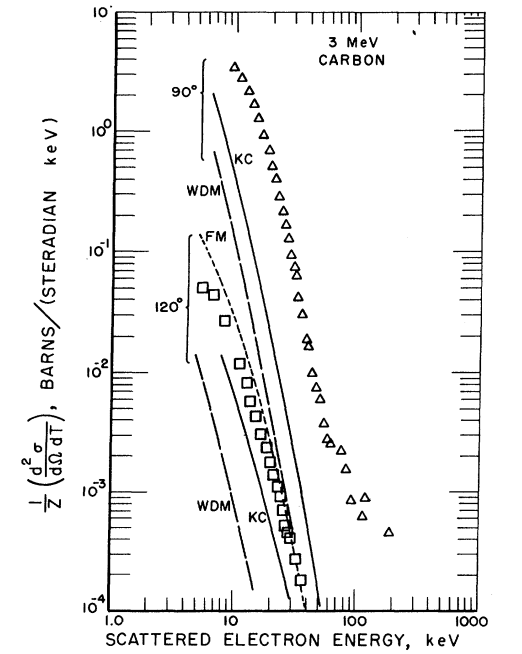

FIG. 16. Comparison of experimental and theoretical inelastic cross sections per atomic electron $(1/Z)\, d^2\sigma/d\Omega\, dT$ for an 11-μg/cm^2 carbon target at 90° and 120° with incident electron energy of 3.0 MeV. The theoretical curves have been evaluated by Kolbenstvedt and Cooper (KC) (Ref. 11) from Eq. (25) given by Weber, Deck, and Mullin (WDM) (Ref. 4) and from Eq. (22) given by Ford and Mullin (FM) (Ref. 3) for multiple scattering.

nates the single-scattering cross sections of WDM and KC. The data at 90° was not compared with FM because of the non-normal incident electron beam direction, but the difference here between the experimental data and the WDM and KC calculations indicates that multiple scattering is even more of a problem, probably because the effective target thickness is greater than at 60° or 120°. Further investigations with atomic-beam targets are necessary to determine whether the agreement with FM is fortuitous or whether multiple-scattering effects are really so important, even for so thin a low-atomic-number target. The other possibility is that the discrepancies between the experimental data and WDM and KC arise because of the breakdown of the plane-wave approximation. This possibility can only be examined after calculations based on exact wave functions become available.

*A preliminary report of this work was given by G. Missoni, R. C. Placious, and J. W. Motz, Bull. Am. Phys. Soc. 13, 898 (1968), Abstract ED 10.

†Present address: Dept. of Physics, University of Bari, Bari, Italy.

[1]Excellent reviews of these studies are given by B. L. Moiseiwitsch and S. J. Smith, Rev. Mod. Phys. 40, 238 (1968); and M. R. H. Ridge, *ibid.* 40, 564 (1968). An excellent review of experimental results is given by L. J. Kieffer and G. H. Dunn, *ibid.* 38, 1 (1966).

[2]C. Møller, Ann. Physik 14, 568 (1932).

[3]G. W. Ford and C. J. Mullin, Phys. Rev. 110, 520 (1958).

[4]T. A. Weber, R. T. Deck, and C. J. Mullin, Phys. Rev. 130, 660 (1963).

[5]J. W. Motz and R. C. Placious, Phys. Rev. 132, 1120 (1963).

[6]C. E. Dick and J. W. Motz, Phys. Rev. 171, 75 (1968).

[7]J. W. Motz, Haakon Olsen, and H. W. Koch, Rev. Mod. Phys. 36, 881 (1964).

[8]K. J. Steffen, *High Energy Beam Optics* (Interscience, New York, 1965), Chap. 3.

[9]M. J. Berger, S. M. Seltzer, S. E. Chappell, J. C. Humphreys, and J. W. Motz, Nucl. Instr. Methods 69, 181 (1969).

[10]References to some of the studies on unfolding procedures for spectral analysis are given by J. B. Birks, *The Theory and Practice of Scintillation Counting* (Macmillan, New York, 1964), p. 492.

[11]J. J. Kepes, B. Waldman, and W. C. Miller, Ann. Phys. (N.Y.) 6, 90 (1959).

[12]H. Kobenstvedt and J. W. Cooper, Phys. Rev. (to be published). This study is expected to be published concomitantly with the present article.

PHYSICAL REVIEW A VOLUME 2, NUMBER 6 DECEMBER 1970

Photoionization of Sodium, Lithium, and Potassium by a Pseudopotential Method*

R. L. Smith and R. W. LaBahn

Department of Physics and Astronomy, Louisiana State University, Baton Rouge, Louisiana 70803

(Received 1 June 1970)

A pseudopotential formalism is used to calculate the cross section for photoionization of sodium, lithium, and potassium for ejected electron energies from threshold to about 15 eV. Both the dipole length and dipole velocity matrix forms are computed. For sodium, the dipole length results are in good agreement with experiment away from the lowest threshold. The dipole velocity results for sodium, on the other hand, severely underestimate the cross section except very near threshold. For lithium, the dipole length and velocity results are less than the experimental results but agree well with other theoretical results. For potassium, the cross section exhibits the general shape of experimental curves.

I. INTRODUCTION

In principle, the cross sections for photoionization can be calculated when accurate wave functions are known for the states of the atoms and ions. In practice, assumptions have to be made in order to obtain the necessary wave functions. In a previous publication by the authors,[1] a pseudopotential formalism was used to calculate the photoionization cross section of sodium. The photoionization cross-section results, using the dipole length form of the matrix, were in very good agreement with experiment. The object of this paper is to extend the work on sodium to include polarization effects and to apply the pseudopotential method to obtain photoionization cross sections of lithium and potassium.

The pseudopotential method[2] has been used extensively in solid-state physics and has only recently been applied to atomic collision processes.[3–6] The general concept of the pseudopotential method is that a valence electron in an atom or a solid sees a weak net effective potential. Inside the core of the atom the nuclear potential acting on a valence electron is very strong and attractive. Also, in this